UWB SAR Imaging of Near-Field Object for Industrial Process Applications

UWB SAR Imaging of Near-Field Object for Industrial Process Applications

Seyedeh Shaghayegh Fayazi*, Jian Yang*, Hoi-Shun Lui†,

*Dept. of Signals and Systems, Chalmers University of Technology
SE-41296 Gothenburg, Sweden, Email: sash0011@student.umu.se, jian.yang@chalmers.se
†School of Information Technology and Electrical Engineering, The University of Queensland
Brisbane, Queensland 4072, Australia, Email: h.lui@uq.edu.au

***Abstract*—Ultra wideband technology becomes more widely used for near-field object detection. We present an aperture synthetic radar (SAR) system using ultra-wideband (UWB) signals for such applications. One of the problems with UWB time-domain SAR imaging algorithm is the artefact originated from scattered field of adjacent objects. In this paper an algorithm based on the Range Point Migration (RPM) method is used to alleviate this problem. This method estimates a possibility distribution of the optimal Direction of Arrival (DOA) of the scattered field from objects. A weighting factor based on this possibility is used to suppress the effect of artifact scattered fields. The results in the paper show that the UWB SAR accompanied with RPM can produce an image of an object with a significant suppression of undesired artifact from scattered field of adjacent objects.**

***Index Terms*—aperture synthetic radar, ultrawide-band, near-field imaging**

I. Introduction

Ultra WideBand (UWB) pulse radar is one of the promising techniques for near-field sensing systems, for examples, automated target recognition in non-contact measurement with a high resolution [1], imaging of buried objects underground [2], [3], UWB indoor and through-wall imaging radar [4], [5], UWB stroke diagnosis system [6], as well as some fundamental investigation of the penetration ability of UWB signals [7]. In many of these applications UWB synthetic aperture radar (SAR) imaging algorithm is used to form an image from the subsurface of the object.

However, one drawback with UWB time-domain SAR imaging algorithm is the undesired blurry image of the true object due to the scattered fields of adjacent objects. Since SAR algorithm is only based on the summation at each pixel of all time-delayed signals coming from all scattered fields, the algorithm cannot distinguish the scattered field of the object at this pixel from those scattering of objects at other pixels. Therefore, this false contribution of some scattered fields to some pixels will produce a false blurry image around the true object, which is referred to as the artifact. We presented a simple solution to the artifact for simple geometries in [8]. However, for more complex objects this simple solution does not work well. Therefore, it is necessary to look for better artifact compensation solutions.

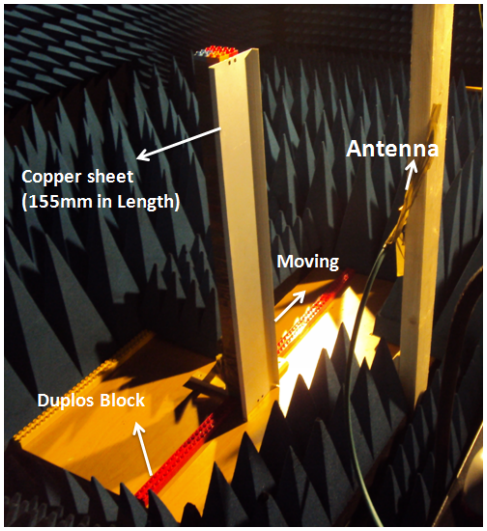

Fig. 1. Experimental setup.

In this study a new algorithm based on Range Point Migration (RPM) method is proposed to reduce such artefact. The RPM estimates an accurate Direction of Arrival (DOA) according to the range point global characteristic [9]. This DOA estimation information, combined with the physical direction of the pixels, can produce a weighting factor and can distinguish the scattering from the object at this pixel from those scattering from other objects.

A. Data Accusation and Experimental Setup

The test setup for the UWB SAR system is shown in Fig. 1, a self-grounded Bow-Tie antenna [10], [11] located in front of a rectangular metal plate. This metal plate is then moved along a path of straight line of 1088 mm long. In order to achieve higher flexibility and accuracy in positioning, this straight line was made of 68 Duplos LEGO Blocks, each with a length of 16 mm. The distance between the antenna and the straight line path is 715 mm. The monostatic response of each of these 68 positions is measured by Vector Network Analyzer (VNA) in frequency domain between 0.5 to 13 GHz, and then, an inverse Fourier Transform is applied to obtain the time domain data.

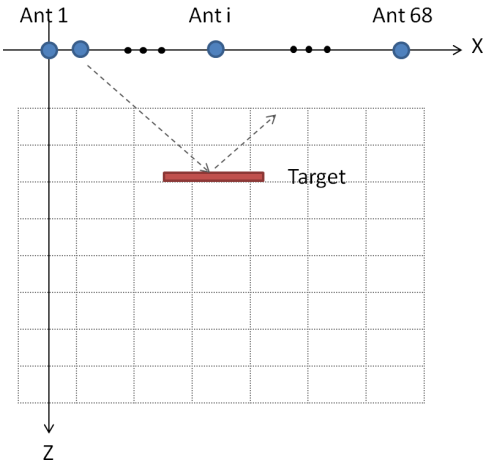

Fig. 2. The principle of the SAR algorithm.

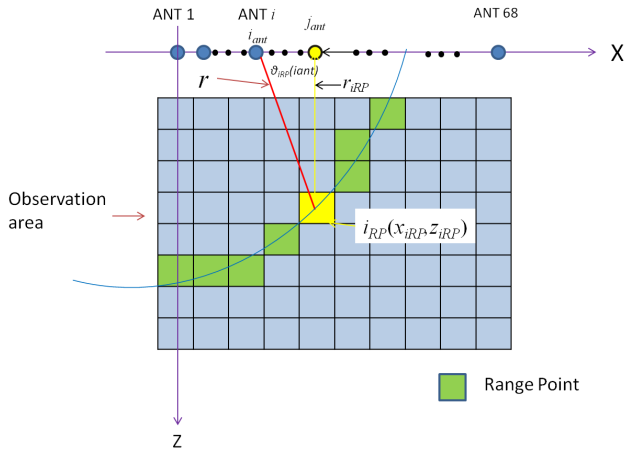

Fig. 3. The principle of RPM algorithm.

All the measurements were done in an anechoic chamber such that the reflection from surrounding environment is minimized.

This setup is equivalent to the case that a single antenna moves along 68 equally spaced positions in front of a static object. Using these 68 monostatic responses in time domain and the SAR imaging algorithm, an image of the object can be formed.

B. Imaging Algorithm Principle

In order to reconstruct an image of the object, which in the case of this study, is a rectangular metal plate with the length of 155 mm shown in Fig 1, the SAR imaging technique in [2], [3] is utilized except that only monostatic responses are used here. As it is described earlier in the SAR geometry, an array of 68 antennas located in front of the object is considered, see Fig 2. The intensity of each pixel $I(m,n)$ is calculated by using

$$I(m,n) = \sum_{k=1}^{K} S_k(t = T_{k,m,n}). \tag{1}$$

where K is the total number of the antennas, S_k is the received signal in time domain at the kth antenna position and $T_{k,m,n}$ is the round-trip time delay between the kth antenna and the physical position represented by pixel (m,n) in the image, see Fig. 2

C. Artefact Concept

In order to reconstruct the image at each pixel, the distance d between this pixel and the antenna is used to calculate the time delay $t_d = 2d/c$, then the signal at this time delay $S(t = t_d)$ is picked up. If the object is present in this pixel, a strong value for $S(t = t_d)$ will be chosen and used in the image (1). However, the signals from other pixels is also picked up if those other pixels have the same distance as that of this pixel to the antenna, which results in an arc-shaped artifact.

D. Direction of Arrival

One method to suppress this arc-shaped artifact is using the directional-of-arrival (DOA) information of the scattered fields at each pixel. One of the promising algorithms for obtaining DOA of scattering with rather complex boundaries is the Range Point Migration (RPM) method [9], [12]. It is obvious that $S(t = t_d)$ will take all scattered fields from all point (x,z) on a circle with the center $(X_{iant}, 0)$ and radius $d/2$, as shown in Fig 3. Therefore, we have to use the signals of the antenna at other positions to obtain the DOA information [9], i.e., to calculate the possibility distribution of DOA (θ_{opt}), referred to as optimal theta range, by

$$\theta_{\text{opt}}(i_{ant}, r) = \left(\arg \max_{0<\theta<\pi} \left| \sum_{i_{(RP=1)}}^{N_{RP}(i_{ant},r)} s_{jant}(r_{iRP}) \exp^{-\left[\frac{(x_{iant}-x_{iRP})^2}{2\sigma_x^2} + \frac{(\theta-\theta_{iRP}(i_{ant}))^2}{2\sigma_\theta^2}\right]} \right| \right) \tag{2}$$

Then, together with the real physical direction θ_p at the pixel for the antenna position, shown in Fig. 4, a weighting factor is obtained to suppress undesired scattered fields producing the arc-shaped artifact, see Figs. 5 and 6.

Assuming the distance between a certain antenna position and a certain pixel is r, all the pixels with this distance r from that antenna are considered as range points for that antenna, see Fig. 3. The angle θ_{iRP}, as shown in the figure, can be calculated by

$$\theta_{\text{iRP}} = \arctan \frac{Z_{iant} - Z_{RP}}{X_{iant} - X_{RP}} \tag{3}$$

S_{jant} is the received signal by the antenna at jth position, where j_{ant} can be calculated by (4). If there is an object at the pixel i_{RP}, S_{jant} should have strong value since the antenna is

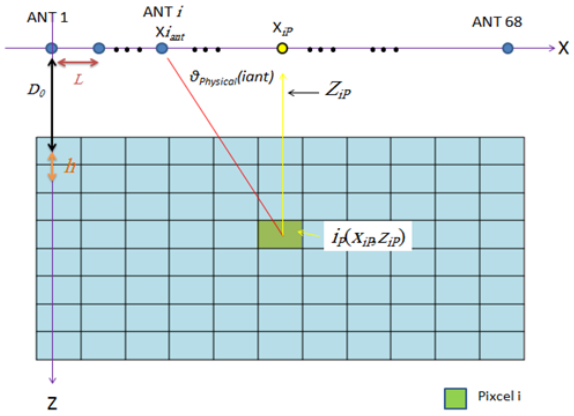

Fig. 4. The geometry of the SAR configuration.

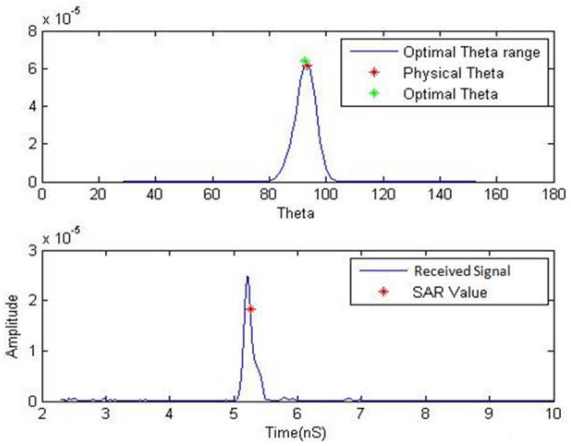

Fig. 5. The object is present in this pixel.

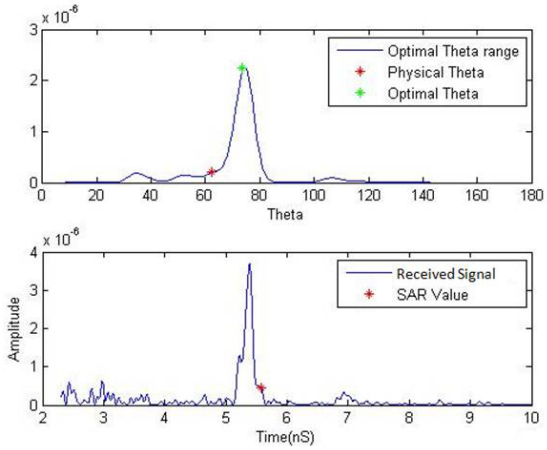

Fig. 6. The smile is present in this pixel.

now located in front of that object, which is clearly observed in Fig 3. r_{iRP} is the distance from the located antenna to that special range pixel.

$$j_{ant} = \arg \min_{1 \le i_{ant} \le k} |x_{iant} - x_{iRP}| \tag{4}$$

The σ_x and σ_θ are constant value and can be determined empirically. Here we use $\sigma_x = 10$ and $\sigma_\theta = \pi$.

E. Physical Theta Calculation

For a certain antenna position and a certain pixel, we can calculate an angle known as physical theta $\theta_{\mathrm{physical}}$ as (shown in Fig 4)

$$\theta_{\mathrm{physical}} = \arctan \frac{Z_{iant} - Z_{ip}}{X_{iant} - X_{ip}} \tag{5}$$

It is clearly observed that if there is an object in the pixel, the ratio of the value of optimal theta range at $\theta_{\mathrm{physical}}$ to the value of optimal theta range at θ_{opt} is close to one, while if there is no object in the pixel, this ratio is close to zero, see Fig 5 and Fig 6.

We use the above mentioned ratio as a weighting factor α in the SAR imaging formula. Hence, the updated intensity $I(m,n)$ of pixel (m,n) is given by

$$I(m,n) = \sum_{k=1}^{K} \alpha \times S_k(t = T_{k,m,n}). \tag{6}$$

Thus, the effect of unnecessary mono-static responses in SAR algorithm can be suppressed.

II. MEASURED RESULTS

The UWB SAR image without using RPM is shown in Fig 7, where the undesirable arc-shaped artefact appears around the rectangular metal plate object.

Fig 8 shows the image of UWB SAR algorithm with RPM. It can be seen that the artefact have been removed.

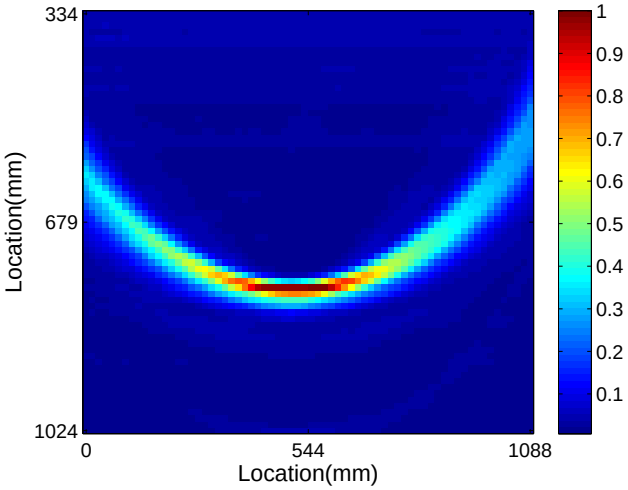

Fig. 7. Image reconstruction results based on SAR algorithm

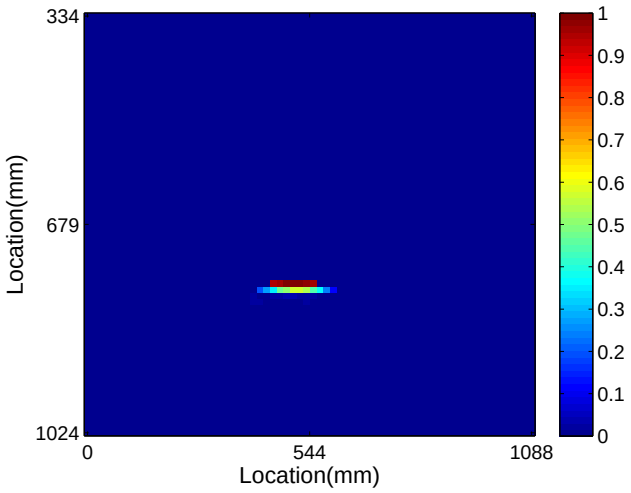

Fig. 8. Final SAR reconstructed Image using RPM method

Some details concerning data treatment are as follows. First, a threshold is applied to the time domain data so that the noise outside the main signal pulse is removed. Then, we perform a scan over pixels. If the intensity of a pixel using SAR without RPM is zero, we conclude that there is no object at this pixel. If the intensity of a pixel using SAR without RPM is not zero, we apply the RPM method to this pixel. By doing so, we obtain the image in a more efficient manner.

III. Conclusion

This paper present a new algorithm for UWB SAR system for near-field imaging in order to suppress the undesirable arc-shaped artefact. The results from experimental data demonstrate that this SAR-and-RPM combined algorithm can suppress artefact in near-field UWB SAR imaging.

Acknowledgment

This work has been supported by CHASE Center at Chalmers University of Technology.

References

[1] H. Lui and N. Shuley, "Radar target identification using a banded E-pulse technique," *IEEE Transactions on Antennas and Propagation*, vol. 54, no. 12, pp. 3874–3881, 2006.

[2] Y. Wang, I. D. Longstaff, and C. J. Leat, "SAR Imaging of Buried Objects from MoM modelled scattered field," *IEE Proc. Radar, Sonar and Navigation*, vol. 148, no. 3, pp. 167–172, 2001.

[3] S. Vitebskiy, L. Carin, M. A. Ressler, and F. H. Le, "Ultra-Wideband, Short-Pulse Ground-Penetrating Radar: Simulation and Measurement," *IEEE Trans. Geoscience and Remote Sensing*, vol. 33, no. 3, pp. 762–772, 1997.

[4] Y. Yu, S. Maalik, J. Yang, T. McKelvey, K. Malmstrom, L. Landén, and B. Stoew, "A new UWB radar system using UWB CMOS chip," in *Proceedings of the 5th European Conference on Antennas and Propagation (EUCAP)*. IEEE, 2011, pp. 771–775.

[5] Y. Yu, J. Yang, T. McKelvey, and B. Stoew, "A compact uwb indoor and through-wall radar with precise ranging and tracking," *International Journal of Antennas and Propagation*, vol. 2012, 2012.

[6] S. Abtahi, J. Yang, and S. Kidborg, "A new compact multiband antenna for stroke diagnosis system over 0.5–3 GHz," *Microwave and Optical Technology Letters*, vol. 54, no. 10, pp. 2342–2346, 2012.

[7] A. Razavi and J. Yang, "Investigation of penetration ability of UWB antennas in near-field sensing applications," in *2012 6th European Conference on Antennas and Propagation (EUCAP)*. IEEE, 2012, pp. 791–795.

[8] S. Fayazi, H. Lui, and J. Yang, "Microwave imaging of near-field object using ultra-wideband synthetic aperture radar algorithm," in *2012 IEEE Antennas and Propagation Society International Symposium (APSURSI)*. IEEE, 2012, pp. 1–2.

[9] S. Kidera, T. Sakamoto, and T. Sato, "Super-Resolution UWB Radar Imaging algorithm Based on Extended Capon With Reference Signal Optimization," *IEEE Trans. Antennas and Propagation.*, vol. 59, no. 5, pp. 1606–1615, 2011.

[10] J. Yang and A. Kishk, "A novel low-profile compact directional ultra-wideband antenna: the self-grounded bow-tie antenna," *IEEE Transactions on Antennas and Propagation*, vol. 60, no. 3, pp. 1214–1220, 2012.

[11] ——, "The self-grounded Bow-Tie antenna." Spokane, Washington: 2011 IEEE AP-S International Symp. on Antennas Propag., 3-8 July 2011.

[12] S. Kidera, T. Sakamoto, and T. Sato, "Accurate UWB Radar 3-D imaging algorithm for complex boundary without range points conections," *IEEE Trans. Geosci.Remote Sens.*, vol. 48, no. 4, pp. 1993–2004, 2010.